The Astrophysical Journal Letters, 894:L8 (6pp), 2020 May 1 https://doi.org/10.3847/2041-8213/ab8af4

Twin Stars and the Stiffness of the Nuclear Equation of State: Ruling Out Strong Phase Transitions below $1.7\,n_0$ with the New NICER Radius Measurements

Jan-Erik Christian and Jürgen Schaffner-Bielich
Institut für Theoretische Physik, Goethe Universität Frankfurt, Max von Laue Strasse 1, D-60438 Frankfurt, Germany; christian@astro.uni-frankfurt.de, schaffner@astro.uni-frankfurt.de
Received 2020 January 17; revised 2020 March 11; accepted 2020 April 16; published 2020 May 1

Abstract

We explore the connection between the stiffness of a hadronic equation of state (EoS) with a sharp phase transition to quark matter to its tidal deformability. For this we employ a hadronic relativistic mean field model with a parameterized effective nucleon mass to vary the stiffness in conjunction with a constant speed of sound EoS for quark matter. We compute multiple scenarios with phase transitions according to the four possible cases of a hybrid star EoS with a stable second branch. We demonstrate how the effective nucleon mass can be constrained by using gravitational-wave data. We find that certain values of the effective nucleon mass are incompatible with GW170817 and a phase transition simultaneously. By using the recent NICER measurements of J0030+0451 we constrain our results further and find that strong phase transitions with a visible jump in the mass–radius relation are ruled out at 1σ at densities below 1.7 times saturation density.

Unified Astronomy Thesaurus concepts: Neutron stars (1108); Compact objects (288)

1. Introduction

Advances in astrophysical observations allow for unprecedented insights into the properties of neutron star matter, the equation of state (EoS). From the inspiral of two compact stars the chirp mass $\mathcal{M}$ and the weighted tidal deformability $\tilde{\Lambda}$ can be measured (Abbott et al. 2017; Bauswein et al. 2017; Annala et al. 2018; Paschalidis et al. 2018). This makes gravitational-wave data useful in constraining the EoS for compact stars. Another important constraint is the maximal observed mass of a neutron star. Currently the highest measured mass for a neutron star is about $2M_\odot$ (Demorest et al. 2010; Antoniadis et al. 2013; Fonseca et al. 2016) or slightly higher at $2.14^{+0.10}_{-0.09}M_\odot$ (Cromartie et al. 2019).

In this work we confront neutron stars composed of nuclear and quark matter, so-called hybrid stars in view of these above-mentioned astrophysical constraints. Hybrid stars (Ivanenko & Kurdgelaidze 1965; Itoh 1970; Alford et al. 2005; Coelho et al. 2010; Chen et al. 2011; Masuda et al. 2013; Yasutake et al. 2014; Zacchi et al. 2016) feature a hadronic mantle and a quark matter core. In contrast to pure hadronic EoSs, which generate a single stable branch in a mass–radius relation, these hybrid EoSs can generate a second stable branch. This can lead to so-called twin stars, where two stars have the same mass, but different radii (Kämpfer 1981; Glendenning & Kettner 2000; Schertler et al. 2000; Schaffner-Bielich et al. 2002; Zdunik & Haensel 2013; Alford et al. 2015; Blaschke & Alvarez-Castillo 2016; Alford & Sedrakian 2017; Zacchi et al. 2017; Christian et al. 2018; Blaschke et al. 2020). These hybrid star EoSs fit well with the low values of tidal deformability measured for GW170817, due to their high compactness (Paschalidis et al. 2018; Alvarez-Castillo et al. 2019; Christian et al. 2019; Montana et al. 2019; Sieniawska et al. 2019). Another method of reconciling the tension between the need for a stiff EoS posed by the $2M_\odot$ constraint and the need for a soft EoS posed by the measurement of GW170817 is the two-family scenario (Drago et al. 2016; Drago & Pagliara 2016, 2018). In this scenario the $2M_\odot$ constraint is fulfilled by a strange quark star branch that coexists with the (soft) hadronic EoS. This scenario permits strong phase transitions even for soft hadronic EoSs.

At present the possibility of pure quark stars cannot be ruled out (Ivanenko & Kurdgelaidze 1965; Itoh 1970; Bodmer 1971; Alcock et al. 1986; Haensel et al. 1986; Fraga et al. 2002; Zacchi et al. 2015), but we are not discussing these special type of compact stars in the following that require the existence of absolutely stable quark matter or the two-family scenario.

In the following we explore the influence of the stiffness and transition parameters of a hadronic EoS featuring a first-order phase transition to quark matter. A widely used approach to describe the hadronic matter in neutron stars is the relativistic mean field model (Johnson & Teller 1955; Duerr 1956; Walecka 1974; Boguta & Bodmer 1977; Serot & Walecka 1986; Mueller & Serot 1996; Typel et al. 2010; Hornick et al. 2018). We employ the parameterizable relativistic mean field EoS by Hornick et al. (2018), which enables us to vary the effective nucleon mass. The effective nucleon mass is linked to the stiffness of the EoS (Boguta & Stöcker 1983), see also Yasin et al. (2020). The phase transition and quark matter EoS is modeled using the constant speed of sound parameterization (Alford et al. 2014). The parameters for the phase transition are chosen according to the four categories of twin stars outlined in Christian et al. (2018). We find that the presence of a phase transition reduces the tidal deformability, making the underlying hadronic EoSs considered to be too stiff compatible with the GW170817 data. However, a soft EoS might not be capable of generating a second branch in the mass–radius relation. This way certain assumptions on a phase transition for a known stiffness of the nuclear EoS can be excluded. The recent measurements by NICER of the pulsar J0030+0451 can be used to constrain the EoS further. Riley at al. state a mass of $1.34^{+0.15}_{-0.16}M_\odot$ with a radius of $12.71^{+1.14}_{-1.19}$ km (Riley et al. 2019), while Miller et al. state $1.44^{+0.15}_{-0.14}M_\odot$ with a radius of $13.02^{+1.24}_{-1.06}$ km (Miller et al. 2019). This constraint rules out a strong phase transition at densities of $n \lesssim 1.7\,n_0$. We show that the NICER data provide an indication that an

extremely soft nuclear EoS and a strong phase transition are mutually exclusive.

2. Theoretical Framework

2.1. EoS

2.1.1. Hadronic EoS

The relativistic parameterization introduced by Todd-Rutel & Piekarewicz (2005; see also: Chen & Piekarewicz 2014; Hornick et al. 2018) is a generalized relativistic mean field approach with the main advantage that the slope parameter L, the symmetry energy J, and the effective nucleon mass m^*/m can be easily adjusted. Taking into account σ, ω, and ρ mesons, the interaction Lagrangian can be written as

$$\begin{aligned}\mathcal{L}_{\rm int} = \sum_N \overline{\psi}_i \left[g_\sigma \sigma - g_\omega \gamma^\mu \omega_\mu - \frac{g_\rho}{2} \gamma^\mu \boldsymbol{\tau} \boldsymbol{\rho}_\mu \right] \psi_i \\ - \frac{1}{3} bm (g_\sigma \sigma)^3 - \frac{1}{4} c (g_\sigma \sigma)^4 \\ + \Lambda_\omega (g_\rho^2 \boldsymbol{\rho}_\mu \boldsymbol{\rho}^\mu)(g_\omega^2 \omega_\mu \omega^\mu) + \frac{\zeta}{4!} (g_\omega^2 \omega_\mu \omega^\mu)^2. \end{aligned} \quad (1)$$

The last two terms describe a density dependence via the σ–ω coupling term Λ_ω and the quadratic self-coupling ζ of the ω mesons (Mueller & Serot 1996; Horowitz & Piekarewicz 2001; Todd-Rutel & Piekarewicz 2005). The g_σ and g_ω couplings can be used to determine the density of the ground state n_0, as well as the binding energy per particle $E/A(n_0)$.

If one wants to determine the values of $E/A(n_0)$, b, c, and Λ_ω one needs to fix certain parameters. Hornick et al. (2018) followed the approach by Chen & Piekarewicz (2014) to do so. Apart from n_0, $E/A(n_0)$, incompressibility $K(n_0)$, the parameters J, L, and m^*/m have to be fixed. In the following the value of ζ is set to zero (Chen & Piekarewicz 2014) to achieve the stiffest possible EoS. K is fixed to $K = 240$ MeV (Hornick et al. 2018). Hornick et al. additionally constrain the parameters using the constraints from χEFT for densities up to $1.3\,n_0$ (Drischler et al. 2016). By comparing the different EoSs with the allowed band from χEFT they find that only values of $40\,\mathrm{MeV} \leqslant L \leqslant 60\,\mathrm{MeV}$ are possible, $30\,\mathrm{MeV} \leqslant J \leqslant 32\,\mathrm{MeV}$.

We fixed the values $L = 60$ MeV and $J = 32$ MeV while varying the effective mass m^*/m. These values of L and J allow for the largest allowed range in effective mass values (see Hornick et al. 2018). We note that the mass–radius relation does not depend significantly on the choices of L and J (Hornick et al. 2018). The softness of an EoS relates to the value of m^*/m, as only m^*/m controls the high-density behavior (Boguta & Stöcker 1983). Lower values of m^*/m generate a stiffer EoS, while high values generate a softer EoS.

2.1.2. Phase Transition

We assume that at high baryonic densities a first-order phase from hadronic to quark matter takes place. This behavior is modeled with a Maxwell construction. The hadronic matter is described by the parameterized EoS (see Hornick et al. 2018), while the constant speed of sound approach (Zdunik & Haensel 2013; Alford et al. 2014; Alford & Han 2016) in the form used by Alford et al. (2014) is employed for the quark matter. This means the entire EoS is given as

$$\epsilon(p) = \begin{cases} \epsilon_{\rm HM}(p) & p < p_{\rm trans} \\ \epsilon_{\rm HM}(p_{\rm trans}) + \Delta\epsilon + c_{\rm QM}^{-2}(p - p_{\rm trans}) & p > p_{\rm trans} \end{cases}, \quad (2)$$

where $p_{\rm trans}$ is the pressure at which the transition takes place and $\epsilon_{\rm HM}(p_{\rm trans})$ is the corresponding energy density. The discontinuity in energy density at the transition is $\Delta\epsilon$. For the speed of sound in the stars core, a value of $c_{\rm QM} = 1$ is assumed, using natural units.

2.2. Classification of Twin Stars

A first-order phase transition gives rise to the phenomenon of "twin stars," which are neutron stars with identical mass, but different radii (Kämpfer 1981; Glendenning & Kettner 2000; Schertler et al. 2000; Schaffner-Bielich et al. 2002; Zdunik & Haensel 2013; Alford et al. 2015; Blaschke & Alvarez-Castillo 2016; Zacchi et al. 2017; Christian et al. 2018). In order to investigate twin star equations of state it can be useful to classify the twin star solutions into four distinct categories, as described in Christian et al. (2018). In this subsection a short summary of the four categories is provided. We refer to the maximum of the hadronic branch as the first maximum and the maximum of the hybrid branch as the second maximum in a twin star mass–radius relation. In Christian et al. (2018) we showed that the mass value of the first and second maximum can be related to values of $p_{\rm trans}$ and $\Delta\epsilon$, respectively. The shape of the second branch is governed by the value of $p_{\rm trans}$, while its position is strongly influenced by the value of $\Delta\epsilon$. High values of $p_{\rm trans}$ lead to high masses in the first maximum and flat second branches. Low values of $\Delta\epsilon$ lead to a second branch near the discontinuity (i.e., a high mass at the second maximum). With this in mind the twin star categories can be defined as follows:

I. Both maxima exceed $2M_\odot$, which implies high values of $p_{\rm trans}$ and a nearly flat second branch.
II. Only the first maximum reaches $2M_\odot$, which again requires a high value of $p_{\rm trans}$.
III. The first maximum is in the range of $2M_\odot \geqslant M_{\rm max_I} \geqslant 1M_\odot$, while the second maximum exceeds $2M_\odot$. Accordingly, the transitional pressure is lower than in the previous categories and the second branch becomes steeper.
IV. Like category III the second maximum exceeds $2M_\odot$; however, the first maximum is below even $1M_\odot$. The second branch is at its steepest slope here.

2.3. Tidal Deformability

The observation of gravitational waves from compact star mergers, as demonstrated for GW170817 detected by the LIGO and Virgo observatories (Abbott et al. 2017), can be used to constrain the EoSs of compact stars, because they contain information on the tidal deformability and chirp mass of the participating neutron stars during the inspiral phase.

The chirp mass can be measured to a very high precision and is closely related to the total mass $M_{\rm total}$ via

$$\mathcal{M} = \left(\frac{q}{(1+q)^2} \right)^{\frac{3}{5}} M_{\rm total}, \quad (3)$$

where q is the mass ratio of the participating stars. For GW170817 the chirp mass was measured as $\mathcal{M} = 1.186^{+0.001}_{-0.001} M_\odot$ (Abbott et al. 2019).

The tidal deformability λ measures the quadrupole deformation Q_{ij} of an object in response to the external tidal field $\mathcal{E}_{ij}$ (Hinderer 2008; Hinderer et al. 2010) in the following form:

$$Q_{ij} = -\lambda \mathcal{E}_{ij}, \tag{4}$$

where λ is related to the more commonly used parameter Λ in the following way:

$$\Lambda = \frac{2k_2}{3C^5} \tag{5}$$

with $k_2 = \frac{3}{2}\lambda R^{-5}$ and $C = M/R$ being the compactness of the star.

The most interesting aspect of Λ for our purposes is that it is dependent on the EoS of the compact star, that is being deformed, and that it can be easily calculated (Hinderer 2008; Hinderer et al. 2010; Postnikov et al. 2010). This can be used to compare the calculated values with the gravitational-wave measurement. However, the inspiral of two compact stars with masses $M_1 \geqslant M_2$ can only reveal a combined value of the tidal deformabilities $\tilde{\Lambda}$. For this reason Λ_1–Λ_2 plots are common, where every value of Λ_1 is assigned a fitting value of Λ_2 based on the precisely measured chirp mass. Depending on the EoS this can lead up to three thin lines in the plot. These lines are a neutron–neutron (NN), neutron–hybrid (NH), and hybrid–hybrid (HH) star line (see for more detail: Christian et al. 2019; Montana et al. 2019). Each dot in these plots indicates a possible pair of merging neutron stars. The gravitational-wave data can then be used to constrain the area in the Λ_1–Λ_2 plot from which the measured signal would have originated. Due to the high mass values of all hybrid stars in category I the LIGO measurement excludes the participation of a category I hybrid star in the GW170817 event (see Christian et al. 2019). Category I EoSs might still be viable. However, using GW170817 data they are identical to the purely hadronic case and will thus not be discussed separately. It is possible to determine a lower limit of $\tilde{\Lambda}$ from the electromagnetic counterpart to GW170817; however, this lower limit is a weak constraint (Kiuchi et al. 2019), therefore we will not consider it in the following. In our model only HH star mergers would have difficulties reaching the value of $\tilde{\Lambda} \simeq 250$ stated by Kiuchi et al. (2019).

3. Tidal Deformability from EoS with Varying Stiffness

In the following we present the Λ_1–Λ_2 plots for a selection of EoSs from the categories II–V, as well as the pure hadronic case, described in Christian et al. (2018), with varying m^*/m using the chirp mass and credibility limits from GW170817 as constraints. The effective mass starts at $m^*/m = 0.55$ and is increased in steps of $m^*/m = 0.05$ to $m^*/m = 0.75$. A slope parameter of $L = 60$ MeV and a symmetry energy of $J = 32$ MeV are fixed. Furthermore, we consider all compact stars taking part in the merger event to have masses of $M_1 \geqslant M_2 \geqslant 1 M_\odot$, as about 1 solar mass is the lower limit predicted for neutron stars born in core-collapse supernovae.

We start with the pure hadronic case in Figure 1. In the left plot are the mass–radius relations and in the right one are the corresponding Λ_1–Λ_2 plots. The 90% and 50% credibility levels by LIGO are added into the figure as a dashed and a dotted black line, respectively (Abbott et al. 2019). Like Hornick et al. (2018) we find that effective masses of $m^*/m \geqslant 0.65$ are compatible with GW170817 data.

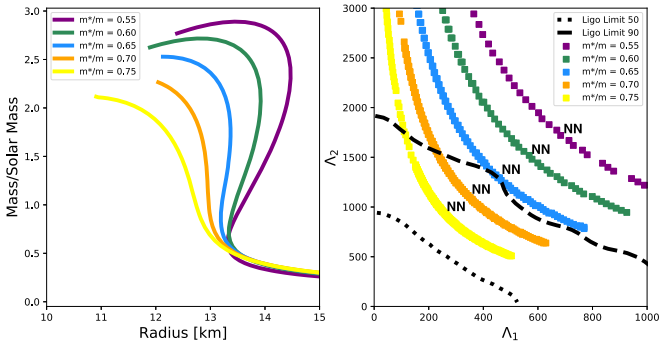

Figure 1. Left: the mass–radius relation for an EoS with $J = 32$ MeV and $L = 60$ MeV, with varied values of m^*/m. Right: the corresponding possible neutron star combinations of the tidal deformability.

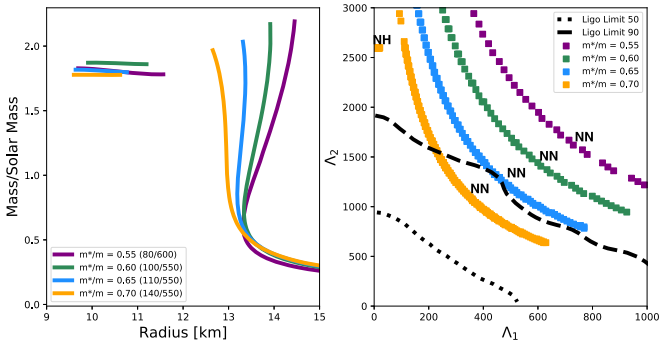

Figure 2. A phase transition of the category II type is depicted; the parameters are written behind the corresponding values of m^*/m in the order $(p_{\text{trans}}/\Delta\epsilon)$ in units of MeV fm^{-3}. The NN combinations are identical to the pure case, due to the late phase transitions. NH combinations close to the axis can be found for all cases. However, the NH combinations are not closer to the LIGO limit than the NN combinations.

Ideally one would keep the parameters of p_{trans} and $\Delta\epsilon$ identical for all variations of m^*/m within a category, in order to investigate the effect of a varied stiffness in isolation. However, in order to find category II solutions high values of p_{trans} and $\Delta\epsilon$ are necessary and due to the high transitional pressure it is not possible to find a single value of p_{trans} that can generate a phase transition for all investigated values of m^*/m. For this reason the p_{trans} and $\Delta\epsilon$ parameters are chosen to be as close together as possible while still generating a category II solution. For a hadronic EoS as soft as the $m^*/m = 0.75$ case it is not possible to find a category II solution at all. The mass–radius relations (left) and the Λ_1–Λ_2 plots (right) from category II are shown in Figure 2.

Only $m^*/m = 0.65$ and $m^*/m = 0.70$ generate NN pairs within the credibility limit of LIGO, as is the case in the purely hadronic scenario. For all category II EoSs the NH pairs are close to the y-axis. This is caused by the high mass values of the hybrid stars in this category. Stiffer hadronic EoSs seem to generate their corresponding NH pairs at higher values of Λ_2. However, even for the softest EoS with $m^*/m = 0.70$ the NH pairs are still above the 90% credibility level. This means, that the compatibility of a category II EoS with GW170817 depends entirely on the hadronic EoS, since only NN combinations are within the LIGO credibility level.

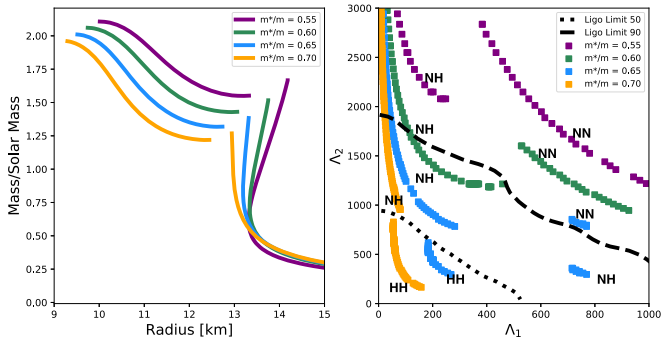

Figure 3. Category III phase transitions with the parameters $p_{\rm trans} = 43$ MeV fm^{-3} and $\Delta\epsilon = 350$ MeV fm^{-3}. There are fewer NN combinations than in the pure case (see Figure 1), since the neutron star branch in the mass–radius relation contains fewer stars. However, the remaining NN combinations do not change their position. The NH combinations and the HH combinations move further into the LIGO credibility limit or closer to it. The $m^*/m = 0.65$ case is a special case, where a single EoS exhibits possible NN, NH, and HH combinations.

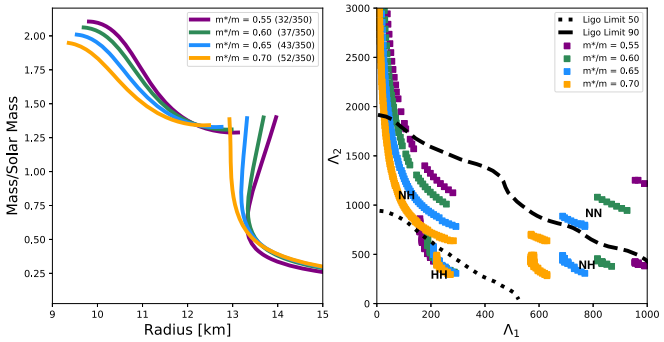

Figure 4. The special case for every considered effective mass. The phase transition is located at the necessary mass to generate HH, NH, and NN combinations for every value of m^*/m, which in the case of GW170817, is roughly $1.4M_\odot$. The parameters are written in the legend in the order ($p_{\rm trans}$/$\Delta\epsilon$) in units of MeV fm^{-3}.

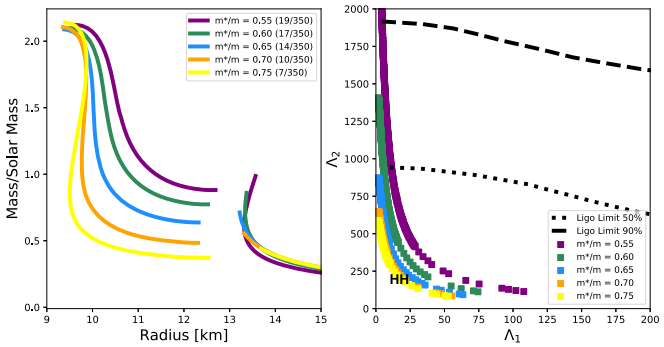

Figure 5. Cases of category IV phase transitions; the parameters are written behind the corresponding values of m^*/m in the order ($p_{\rm trans}/\Delta\epsilon$) in units of MeV fm^{-3}. Category IV is dominated by the EoS describing quark matter. As a result the second branch is stiff and the effective mass has virtually no impact on the EoS. Since only hybrid stars can be combined with other hybrid stars to find the possible areas in the Λ_1–Λ_2 plot in the right panel the possible combinations are very close to each other, even though their mass–radius relations (in the left panel) appear to be very different.

The values $p_{\rm trans} = 43$ MeV fm^{-3} and $\Delta\epsilon = 350$ MeV fm^{-3} can generate category III solutions for all values of m^*/m considered. This is depicted in Figure 3. The stiffest EoS is completely outside of the LIGO credibility level. However, even for the stiffest case the NH pairs are closer to the credibility limit than the pure NN case. The $m^*/m = 0.60$ EoS is the first case where the phase transition improves the compatibility of an EoS with the LIGO measurement by moving some NH combinations into the 90% credibility area, where the pure NN case would be outside of it.

In our previous publication (Christian et al. 2019) we found a special case for a transition at values of $p_{\rm trans} = 43$ MeV fm^{-3} and $\Delta\epsilon = 350$ MeV fm^{-3}, where NN, NH, and HH combinations were generated by a single EoS. The NH pairs are located in two areas, one above the $\Lambda_1 = \Lambda_2$ limit and one below. The latter case is generated by so-called rising twins, where the more massive twin star has a larger radius (Schertler et al. 2000). The hadronic EoS in that case was the DD2 equation by Typel et al. (2010), which has an effective nucleon mass of $m^*/m = 0.6255$. A similar special case can be found for the EoS covered in this work, for an effective mass of $m^*/m = 0.65$. However, if so desired a special case can be realized for any category III EoS, if the transition parameters are chosen accordingly (see Figure 4). The NN pairs of the $m^*/m = 0.65$ case are already at the border of the credible area and the NH pairs can move even further into it. The HH pairs of the $m^*/m = 0.65$ reach below even the 50% credibility limit. The $m^*/m = 0.70$ case does not exhibit NN combinations, but the NH pairs are located nearly completely in the credibility limit, while the HH pairs are below the 50% credibility limit. The $m^*/m = 0.75$ case is missing, because it is not possible to reach the $2M_\odot$ requirement with a category III phase transition.

In contrast to the previous categories it is not difficult to find an EoS in category IV that produces combinations inside the 50% credibility limit. This is because the early phase transition makes the quark matter EoS more dominant and this EoS was chosen specifically to be the most stiffest possible equation consistent with causality. Due to the identical quark matter EoS in all cases we chose to depict different phase transition parameters in Figure 5, as similar values would generate mass–radius relations that are nearly on top of each other. Still, the resulting combinations in the the Λ_1–Λ_2 plot are close together (see the right panel of Figure 5). By definition it is only possible to find HH lines in a category IV case. In Table 1 the compatibility of the four categories with GW170817 in dependence on the effective nucleon mass m^*/m is summarized. In the table category I is written down as I/0, where 0 means "no category." The "x" symbol marks cases where a phase transition fulfills the $2M_\odot$ constraint, but no combinations of neutron stars are located within the LIGO credibility limit. The "y" symbol marks cases where any combination is located within the credibility limit. The "o" is used when the most compact pairs are directly at the credibility limit. A phase transition of category I does not change the compatibility of any of the hadronic EoSs with the GW170817 data, which

Table 1
The Cases of m^*/m and Their Relation to the Tidal Deformability Constraint

Category	0.55	0.60	0.65	0.70	0.75
I/0	x	x	o	y	y
II	x	x	o	y	n.a.
III	y	y	y	y	n.a.
IV	y	y	y	y	y

Note. The "o" denotes the cases where the line is at the 90% credibility limit, "y" is below, and "x" is above.

means that only the $0.65 \leqslant m^*/m \leqslant 0.75$ cases are within the credibility limit, with $m^*/m = 0.65$ at its very border.

The same is true for a category II phase transition. However, it is important to stress that only effective nucleon masses of $m^*/m \leqslant 0.70$ can be realized with a category I or II phase transition. The $m^*/m = 0.75$ case is too soft to generate a stable second branch at the high values of $p_{\rm trans}$ required for the first two categories. A phase transition of category III can lead to NH and HH combinations within the LIGO credibility limit for the $m^*/m \leqslant 0.70$ case. This means that the $m^*/m = 0.70$ case is the only case that can generate NN and NH pairs that are completely within the credibility limit. The $m^*/m = 0.75$ case cannot be realized with a phase transition that generates a stable second branch. However, this configuration cannot be considered a category III case, as the second branch cannot reach $2M_\odot$. It is only possible to find an $m^*/m = 0.75$ case that generates a second branch and has a maximal mass that exceeds $2M_\odot$ if the first branch has its maximum below $1M_\odot$. This means that all cases of m^*/m can generate a stable second branch in the form of a category IV phase transition. Category IV phase transitions generate only HH combinations; these combinations are very compact and as a result all examined cases of m^*/m are within the 50% credibility limit. However, due to the early phase transition the influence of m^*/m on the mass–radius relation is negligible. As a result no meaningful statement about the influence of the effective nucleon mass on a category IV phase transition can be made.

4. A Nicer View on Twin Stars

The recently released mass and radius measurements of the pulsar J0030+0451 by the NICER program (Miller et al. 2019; Raaijmakers et al. 2019; Riley et al. 2019) can be used to constrain the EoSs discussed previously. NICER measures neutron star radii by observing hotspots on the pulsars surface. Depending on the model used to place these hotspots, two different masses and radii are determined. Riley at al. find a mass of $1.34^{+0.15}_{-0.16}M_\odot$ with a radius of $12.71^{+1.14}_{-1.19}$ km (Riley et al. 2019), while Miller et al. find a mass of $1.44^{+0.15}_{-0.14}M_\odot$ with a radius of $13.02^{+1.24}_{-1.06}$ km (Miller et al. 2019). The compactness is determined more precisely and in both cases given as $MG/Rc^2 = 0.16 \pm 0.01$.

In Figure 6 a sample of category III EoSs is depicted, with the constraints from NICER shaded gray and the $2M_\odot$ constraint from J0740+6620 (Cromartie et al. 2019) shaded green. We find that for the pure hadronic cases, all considered effective masses generate neutron stars that fit within the mass–radius range determined by Miller et al. (2019). The $m^*/m \geqslant 0.55$ cases are within the range determined by Riley et al. (2019) as well, only the $m^*/m = 0.55$ case is outside the range.

By definition, only category II–IV phase transitions can support hybrid stars that fulfill the NICER constraints. Category I has to meet the constraints with its hadronic branch. However, category II phase transitions generate massive hybrid stars, which usually are at higher masses than the constraint as well. Category III phase transitions take place at a mass range that is within the NICER likelihood. As a result hybrid stars and pure hadronic stars that fit within the constraint can be found for all effective nucleon masses. The black straight lines in Figure 6 indicate the maximum of the hadronic branch. The lowest maximal masses are generated by the lowest transitional pressures of the respective cases. The $m^*/m = 0.75$ case cannot reach the $2M_\odot$ constraint, as mentioned previously;

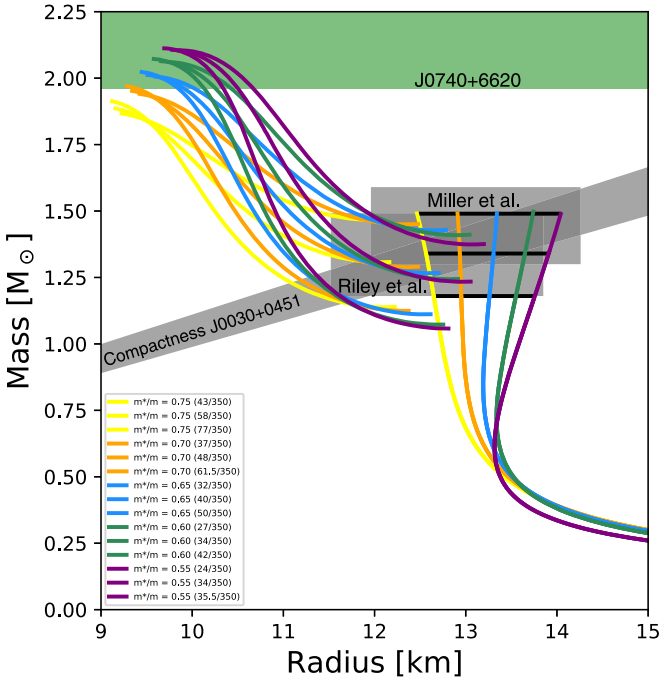

Figure 6. Mass–radius relations for category III phase transitions for all considered effective nucleon masses. The constraints for the J0030+0451 measurement by NICER are taken from Riley et al. (2019) and Miller et al. (2019) and are shaded gray. The $2M_\odot$ constraint from J0740+6620 (Cromartie et al. 2019) is shaded green. All cases of m^*/m can generate neutron stars and hybrid stars within the NICER likelihood, if the transition parameters are chosen accordingly. The $m^*/m = 0.75$ case does not meet the $2M_\odot$ constraint if a phase transition takes place. The black straight lines indicate the maximal mass of the hadronic branch for the respective transitional pressure.

however, the pure hadronic $m^*/m = 0.75$ case fits well with the Riley et al. mass and radius data (Riley et al. 2019).

Due to the comparatively small uncertainty in radius category IV phase transitions that generate neutron stars within the constraints from either Riley et al. or Miller et al. are impossible to find. The hadronic branch ends before the minimal mass is reached. The hybrid star branch would be located at smaller radii than required. This behavior can be seen for the earliest phase transitions of the category III examples in Figure 6 as well. Therefore we can state that a strong phase transition is only compatible with the NICER constraints if the maximal mass of the hadronic branch is greater than the minimal mass of the NICER measurement. This can be related to the transitional pressure and the density. We find that strong phase transitions are not viable for densities below $n \lesssim 1.7\,n_0$. We consider phase transitions "strong" if $\Delta\epsilon \geqslant 350\text{MeV fm}^{-3}$. This value is the lowest value for a discontinuity in energy density that generates a visible difference between the hadronic maximum and the hybrid star minimum of about $0.1M_\odot$ for category IV cases. We used the explicit radii from Riley et al. (2019) and Miller et al. (2019) instead of the corresponding likelihood ellipses. When considering the 2σ likelihood ellipses (Raaijmakers et al. 2019) the constraints become weaker. However, a phase transition with parameters $n \lesssim 1.4n_0$ and $\Delta\epsilon \geqslant 350\text{MeV fm}^{-3}$ is still outside the 2σ likelihood constraints from the NICER measurement.

5. Conclusion

By employing a parameterized relativistic mean field EoS we explored how the stiffness of a hadronic EoS influences the

tidal deformability of an EoS featuring a phase transition from hadronic to quark matter. These phase transitions are chosen to represent the four categories of twin stars (Christian et al. 2018). As stated in our previous work (Christian et al. 2019), an EoS with a phase transition can generate HH, NH, and NN combinations, depending on the location of the phase transition in the mass–radius relation. We consider effective nucleon masses from $m^*/m = 0.75$ to $m^*/m = 0.55$, where a larger effective mass corresponds to a softer EoS. Like Hornick et al. (2018), we find that only the pure hadronic cases for $m^*/m \geqslant 0.65$ are compatible with the GW170817 data (Abbott et al. 2019). The $m^*/m = 0.75$ case is too soft to generate a stable second branch that fulfills the requirement for a category I, II, or III phase transition. Future measurements of neutron stars with masses above $2M_\odot$ might cause similar problems for the $m^*/m = 0.70$ case. At the time of this work the maximal masses of the $m^*/m = 0.70$ category II and III phase transitions are still within the margin of error of the most massive know neutron stars (Demorest et al. 2010; Antoniadis et al. 2013; Fonseca et al. 2016; Cromartie et al. 2019).

Due to the higher compactness of hybrid stars, the $m^*/m \leqslant 0.70$ cases can generate neutron star pairs, from a category III phase transition, deeper within the credibility limit than they could without a phase transition. This means that even the $m^*/m = 0.55$ and $m^*/m = 0.60$ cases, which are on their own too stiff to allow for pairs of neutron stars with sufficiently small values of tidal deformability, can generate combinations within the credibility limit. The benefits of a phase transition in regards to an EoS's compatibility with the LIGO data have been shown before (Paschalidis et al. 2018; Alvarez-Castillo et al. 2019; Christian et al. 2019; Montana et al. 2019).

Only category IV can be realized for all examined values of m^*/m, because the resulting EoSs can be considered independent from m^*/m due to the early phase transition. However, the recent results from NICER (Raaijmakers et al. 2019) are incompatible with a category IV phase transition and furthermore exclude strong phase transitions at densities of $n \lesssim 1.7\, n_0$, where a visible jump in mass of $\Delta M \geqslant 0.1 M_\odot$ at the point of transition occurs.

These results are reached for the stiffest possible quark matter EoS, which achieves the broadest range of results. A softer quark matter EoS would lead to a second branch with a lower maximal mass. This poses problems for category IV phase transitions as they fail to meet the $2M_\odot$ constraint. For instance, an EoS with a speed of sound $c_s^2 = 0.64$ cannot generate a hybrid star with $2M_\odot$ when a strong phase transition takes place before the hadronic branch reaches roughly $1.3M_\odot$. Only if the branches are connected is it possible to generate a $2M_\odot$ hybrid star.

The authors thank Andreas Zacchi for helpful discussions. J. S. acknowledges support from the Helmholtz International Center for FAIR (HIC for FAIR). J.E.C. is a recipient of the Carlo and Karin Giersch Scholarship of the Giersch foundation.

References

Abbott, B. P., Abbott, R., Abbott, T. D., et al. 2017, PhRvL, 119, 161101
Abbott, B. P., Abbott, R., Abbott, T. D., et al. 2019, PhRvX, 9, 011001
Alcock, C., Farhi, E., & Olinto, A. 1986, ApJ, 310, 261
Alford, M., Braby, M., Paris, M., & Reddy, S. 2005, ApJ, 629, 969
Alford, M. G., Burgio, G. F., Han, S., Taranto, G., & Zappalà, D. 2015, PhRvD, 92, 083002
Alford, M. G., & Han, S. 2016, EPJA, A52, 62
Alford, M. G., Han, S., & Prakash, M. 2014, JPSCP, 1, 013041
Alford, M. G., & Sedrakian, A. 2017, PhRvL, 119, 161104
Alvarez-Castillo, D. E., Blaschke, D. B., Grunfeld, A. G., & Pagura, V. P. 2019, PhRvD, 99, 063010
Annala, E., Gorda, T., Kurkela, A., & Vuorinen, A. 2018, PhRvL, 120, 172703
Antoniadis, J., Freire, P. C., Wex, N., et al. 2013, Sci, 340, 6131
Bauswein, A., Just, O., Janka, H.-T., & Stergioulas, N. 2017, ApJL, 850, L34
Blaschke, D., & Alvarez-Castillo, D. E. 2016, in AIP Conf. Proc. 1701, ed. A. Andrianov et al. (Melville, NY: AIP) 020013
Blaschke, D., Alvarez-Castillo, D. E., Ayriyan, A., et al. 2020, in Topics on Strong Gravity, ed. C. A. Zen Vasconcellos (Singapore: World Scientific), 207
Bodmer, A. R. 1971, PhRvD, 4, 1601
Boguta, J., & Bodmer, A. R. 1977, NuPhA, A292, 413
Boguta, J., & Stöcker, H. 1983, PhLB, 120, 289
Chen, H., Baldo, M., Burgio, G., & Schulze, H.-J. 2011, PhRvD, 84, 105023
Chen, W.-C., & Piekarewicz, J. 2014, PhRvC, 90, 044305
Christian, J.-E., Zacchi, A., & Schaffner-Bielich, J. 2018, EPJA, A54, 28
Christian, J.-E., Zacchi, A., & Schaffner-Bielich, J. 2019, PhRvD, 99, 023009
Coelho, J., Lenzi, C., Malheiro, M., Marinho, R. M., & Fiolhais, M., J. 2010, IJMPD, D19, 1521
Cromartie, H. T., Fonseca, E., Ransom, S. M., et al. 2019, NatAs, 4, 72
Demorest, P., Pennucci, T., Ransom, S., Roberts, M., & Hessels, J. 2010, Natur, 467, 1081
Drago, A., Lavagno, A., Pagliara, G., & Pigato, D. 2016, EPJA, A52, 40
Drago, A., & Pagliara, G. 2016, EPJA, A52, 41
Drago, A., & Pagliara, G. 2018, ApJL, 852, L32
Drischler, C., Carbone, A., Hebeler, K., & Schwenk, A. 2016, PhRvC, 94, 054307
Duerr, H.-P. 1956, PhRv, 103, 469
Fonseca, E., Pennucci, T. T., Ellis, J. A., et al. 2016, ApJ, 832, 167
Fraga, E. S., Pisarski, R. D., & Schaffner-Bielich, J. 2002, NuPhA, A702, 217
Glendenning, N. K., & Kettner, C. 2000, A&A, 353, L9
Haensel, P., Zdunik, J. L., & Schaeffer, R. 1986, A&A, 160, 121
Hinderer, T. 2008, ApJ, 677, 1216
Hinderer, T., Lackey, B. D., Lang, R. N., & Read, J. S. 2010, PhRvD, 81, 123016
Hornick, N., Tolos, L., Zacchi, A., Christian, J.-E., & Schaffner-Bielich, J. 2018, PhRvC, 98, 065804
Horowitz, C. J., & Piekarewicz, J. 2001, PhRvC, 64, 062802
Itoh, N. 1970, PThPh, 44, 291
Ivanenko, D. D., & Kurdgelaidze, D. F. 1965, Ap, 1, 251
Johnson, M. H., & Teller, E. 1955, PhRv, 98, 783
Kämpfer, B. 1981, JPhA, A14, L471
Kiuchi, K., Kyutoku, K., Shibata, M., & Taniguchi, K. 2019, ApJL, 876, L31
Masuda, K., Hatsuda, T., & Takatsuka, T. 2013, ApJ, 764, 12
Miller, M. C., Lamb, F. K., Dittmann, A. J., et al. 2019, ApJL, 887, L24
Montana, G., Tolos, L., Hanauske, M., & Rezzolla, L. 2019, PhRvD, 99, 103009
Mueller, H., & Serot, B. D. 1996, NuPhA, A606, 508
Paschalidis, V., Yagi, K., Alvarez-Castillo, D., Blaschke, D. B., & Sedrakian, A. 2018, PhRvD, 97, 084038
Postnikov, S., Prakash, M., & Lattimer, J. M. 2010, PhRvD, 82, 024016
Raaijmakers, G., Riley, T. E., Watts, A. L., et al. 2019, ApJL, 887, L22
Riley, T. E., Watts, A. L., Bogdanov, S., et al. 2019, ApJL, 887, L21
Schaffner-Bielich, J., Hanauske, M., Stöcker, H., & Greiner, W. 2002, PhRvL, 89, 171101
Schertler, K., Greiner, C., Schaffner-Bielich, J., & Thoma, M. H. 2000, NuPhA, A677, 463
Serot, B. D., & Walecka, J. D. 1986, AdNuP, 16, 1
Sieniawska, M., Turczanski, W., Bejger, M., & Zdunik, J. L. 2019, A&A, 622, A174
Todd-Rutel, B. G., & Piekarewicz, J. 2005, PhRvL, 95, 122501
Typel, S., Röpke, G., Klähn, T., Blaschke, D., & Wolter, H. H. 2010, PhRvC, 81, 015803
Walecka, J. D. 1974, AnPhy, 83, 491, (N.Y.)
Yasin, H., Schäfer, S., Arcones, A., & Schwenk, A. 2020, PhRvL, 124, 092701
Yasutake, N., Lastowiecki, R., Benic, S., et al. 2014, PhRvC, 89, 065803
Zacchi, A., Hanauske, M., & Schaffner-Bielich, J. 2016, PhRvD, 93, 065011
Zacchi, A., Stiele, R., & Schaffner-Bielich, J. 2015, PhRvD, 92, 045022
Zacchi, A., Tolos, L., & Schaffner-Bielich, J. 2017, PhRvD, 95, 103008
Zdunik, J., & Haensel, P. 2013, A&A, 551, A61